Valeology: International Journal of Medical Anthropology and Bioethics
(ISSN 2995-4924) VOLUME 03 ISSUE 7, 2025

PLATINUM-TITANIUM OXIDE NANOPARTICLES AS A SYNERGISTIC RADIOSENSITIZER AND PHOTOTHERMAL AGENT FOR TREATMENT-RESISTANT GLIOBLASTOMA

Muna Khalifa Ali
Department of Physiology and Medical Physics, College of Medicine, Fallujah University, Iraq

Abstract:

Glioblastoma is a highly aggressive and treatment-resistant brain tumor characterized by poor prognosis and limited therapeutic success. This study explored the potential of platinum-core titanium oxide-shell nanoparticles as a dual-function therapeutic agent combining radiosensitization and photothermal therapy. Nanoparticles were synthesized using a two-step process and characterized by DLS, zeta potential, XRD, and FTIR analyses, confirming monodisperse, stable, and crystalline core–shell structures. In vitro cytotoxicity was assessed via MTT assay, demonstrating significant dose- and time-dependent reductions in glioblastoma cell viability. Reactive oxygen species (ROS) levels measured by DCFH-DA fluorescence assay indicated nanoparticle-induced oxidative stress, a likely contributor to the observed cytotoxic effects. Furthermore, survival fraction assays incorporating nanoparticle treatment with radiotherapy (2 Gy X-ray) and near-infrared photothermal stimulation revealed a synergistic effect, achieving the greatest reduction in cell survival when all three modalities were combined. Statistical analysis confirmed the significance of these outcomes. These findings underscore the potential of platinum-titanium oxide core–shell nanoparticles as a promising combinational therapy platform for overcoming radioresistance in glioblastoma. The multifunctionality of the nanoplatform, along with its biocompatibility and physicochemical stability, supports its continued development for translational cancer nanomedicine.

Introduction

Glioblastoma is the most aggressive and lethal primary brain tumor in adults, with median survival rates rarely exceeding 15 months despite maximal surgical resection, chemoradiotherapy, and adjuvant care (Goenka et al., 2021). Resistance to standard treatments, especially radiotherapy, arises from multiple factors including hypoxia, DNA repair mechanisms, and glioma stem-like cells (Chédeville & Madureira, 2021). These resistance mechanisms contribute to the near-universal recurrence of glioblastoma within months of initial therapy, often with a more aggressive and therapy-refractory phenotype (Wang et al., 2023). Recent work has also shown that protective autophagy and efficient DNA repair under radiation stress promote tumor cell survival, complicating the effectiveness of radiotherapy (Xu et al., 2021). Innovative strategies are urgently needed as current treatments fail to overcome the radioresistance conferred by tumor heterogeneity and the glioblastoma microenvironment (Yang et al., 2025).

Nanoparticles offer precise tumor targeting, enhanced permeability, and the ability to overcome resistance through controlled drug release and localized therapeutic activation (Wu et al., 2020). Their ability to function as radiosensitizers stems from high atomic number materials like gold or platinum, which enhance X-ray absorption and intensify radiation-induced DNA damage (Xiang et al., 2020). Photothermal therapy, driven by near-infrared-absorbing nanostructures, allows for non-invasive, site-specific heating and tumor ablation while minimizing systemic toxicity (Chen et al., 2023). Core–shell architectures enable multifunctionality, combining radiosensitization, photothermal heating, and targeted delivery in a single nanoplatform with enhanced stability and responsiveness (Liu et al., 2020). Platinum-titanium oxide combinations are especially promising, merging platinum's radiosensitizing effects with titanium oxide's photothermal potential, offering dual-attack strategies against resistant cancers (Shao et al., 2020).

The objective of this study was to evaluate the therapeutic potential of platinum-core titanium oxide-shell nanoparticles as a dual-function agent for enhancing the treatment of resistant glioblastoma. We aimed to investigate whether the synthesized nanoparticles could synergistically improve the effectiveness of conventional radiotherapy by acting as radiosensitizers while simultaneously inducing photothermal cytotoxicity under near-infrared laser exposure. The study sought to determine the physicochemical properties of the nanoparticles and to assess their biocompatibility, cellular uptake, and ability to generate reactive oxygen species upon radiation exposure. Furthermore, the research aimed to explore the extent to which these nanoparticles could amplify DNA damage and apoptosis in glioblastoma cells compared to radiation treatment alone. Finally, we intended to evaluate the in vivo therapeutic efficacy of the nanoparticles through measurements of tumor growth inhibition and survival outcomes, without the use of imaging technologies, relying solely on direct caliper measurements, biochemical assays, and survival tracking.

Metodology

Nanoparticle Synthesis and Preparation

Platinum-core titanium oxide-shell nanoparticles were synthesized using a two-step controlled process. Initially, colloidal platinum nanoparticles were prepared by reducing chloroplatinic acid (H_2PtCl_6) with sodium borohydride ($NaBH_4$) in an aqueous medium under constant stirring at 4°C. Polyvinylpyrrolidone (PVP) was employed as a stabilizing agent to prevent aggregation during nanoparticle formation. The platinum nanoparticle suspension was then centrifuged and washed several times with deionized water to remove residual reactants.

Following purification, the platinum nanoparticle cores were used as templates for titanium oxide shell growth. A sol-gel method was utilized, where a titanium precursor, titanium isopropoxide

(TTIP), was slowly added to an ethanol-water mixture containing the platinum cores under nitrogen atmosphere. The pH of the solution was carefully adjusted to mildly acidic conditions to promote controlled hydrolysis and condensation of TTIP around the platinum cores. The mixture was stirred continuously for 12 hours to ensure uniform shell formation. Afterward, the resulting platinum-core titanium oxide-shell nanoparticles were collected by centrifugation and washed thoroughly with ethanol and deionized water to remove any unreacted precursors.

The nanoparticles were then subjected to a mild heat treatment at 150°C for 2 hours in an inert argon atmosphere to stabilize the titanium oxide shells without compromising the core integrity. The dried nanoparticles were stored in a desiccator at room temperature until further use. All synthesis steps were conducted under sterile conditions to maintain sample purity for biological experiments.

Dynamic Light Scattering (DLS) Analysis for Particle Size and Size Distribution

Dynamic light scattering was employed to evaluate the hydrodynamic diameter and size distribution profile of the synthesized platinum-core titanium oxide-shell nanoparticles. Measurements were conducted using a Malvern Zetasizer Nano ZS instrument equipped with a 633 nm laser at a scattering angle of 173°, operating under ambient temperature conditions. Prior to analysis, the nanoparticles were dispersed in deionized water to achieve a final concentration of 0.1 mg/mL and sonicated for 10 minutes to minimize aggregation. Each sample was equilibrated for 2 minutes before measurement to ensure thermal stability and homogeneous particle suspension.

For each batch, three independent measurements were performed, and the mean particle size, polydispersity index (PDI), and standard deviation were recorded. The PDI value was used to assess the uniformity of the size distribution, with values below 0.2 considered indicative of a monodisperse system. Instrumental settings, such as refractive index and viscosity, were adjusted according to the properties of water at 25°C to ensure accurate size determination. Data were collected as intensity-weighted distributions and processed using the instrument's built-in software, yielding particle size distribution histograms and cumulative size curves.

The results obtained from DLS were later compared with size information derived from transmission electron microscopy to verify consistency between hydrodynamic and core-shell structural measurements, although the DLS analysis inherently accounted for the hydration layer surrounding each nanoparticle, resulting in slightly larger apparent diameters than those observed by direct imaging methods.

Zeta Potential Measurement for Surface Charge Characterization

The surface charge of the synthesized platinum-core titanium oxide-shell nanoparticles was assessed through zeta potential measurements using a Malvern Zetasizer Nano ZS instrument equipped with a 633 nm laser source. Prior to analysis, nanoparticles were suspended in deionized water at a concentration of 0.1 mg/mL and sonicated for 5 minutes to ensure uniform dispersion. Measurements were conducted at 25°C in disposable folded capillary cells, and all samples were equilibrated thermally for two minutes before the start of data acquisition to eliminate convection effects.

Each batch of nanoparticles was measured in triplicate, and the electrophoretic mobility was automatically converted into zeta potential values by the instrument software using the Smoluchowski equation. The dispersant properties, including refractive index, viscosity, and dielectric constant, were set according to the parameters of deionized water at room temperature. Care was taken to minimize any bubble formation or sedimentation, which could influence the measurement accuracy.

Data were recorded as mean zeta potential values with corresponding standard deviations, and individual distributions were also assessed to confirm the absence of secondary populations or

multimodal charge characteristics. The measurements provided critical insights into the colloidal stability of the nanoparticle suspensions, as zeta potential values with absolute magnitudes above 30 mV are generally associated with electrostatically stable systems. The resulting surface charge data were used not only to evaluate suspension stability but also to infer potential interactions with biological environments during subsequent in vitro and in vivo studies.

X-ray Diffraction (XRD) Analysis for Crystalline Phase Identification

The crystalline structure of the synthesized platinum-core titanium oxide-shell nanoparticles was analyzed using an X-ray diffractometer (Rigaku Ultima IV) equipped with a Cu-Kα radiation source (λ = 1.5406 Å). Samples were prepared by depositing freeze-dried nanoparticles onto low-background silicon sample holders and gently pressing to form a smooth thin layer. Measurements were conducted at room temperature under ambient conditions. The scanning range was set between 20° and 80° 2θ with a step size of 0.02° and a scanning rate of 2° per minute to ensure accurate peak resolution.

The obtained diffraction patterns were compared against standard reference patterns from the Joint Committee on Powder Diffraction Standards (JCPDS) database. Crystalline phases were identified based on the position and relative intensity of characteristic diffraction peaks. The crystallite size of the platinum core and the titanium oxide shell was estimated using the Scherrer equation applied to the full width at half maximum (FWHM) of the most intense peaks for each component. Care was taken to correct for instrumental broadening by measuring a standard silicon sample under the same conditions.

Peak analysis was performed using OriginPro software, with background subtraction and Lorentzian fitting applied to each diffraction peak to determine accurate peak positions and widths. Particular attention was given to distinguishing between the platinum peaks associated with a face-centered cubic (FCC) lattice and the anatase-phase titanium oxide peaks characterized by a tetragonal crystal structure. No additional peaks corresponding to impurity phases were observed, indicating the successful synthesis of pure core-shell nanoparticles with high crystallinity.

Fourier-Transform Infrared Spectroscopy (FTIR) for Surface Chemical Bond Analysis

The surface chemical properties of the synthesized platinum-core titanium oxide-shell nanoparticles were analyzed using Fourier-transform infrared (FTIR) spectroscopy. Spectra were recorded on a Thermo Scientific Nicolet iS10 spectrometer operating in the attenuated total reflectance (ATR) mode. Samples were prepared by drying nanoparticle suspensions at room temperature and depositing the resulting powders onto the ATR crystal without additional treatment. Each spectrum was collected over a wavenumber range of 4000 to 400 cm^{-1} at a resolution of 4 cm^{-1}, with an average of 64 scans per sample to enhance the signal-to-noise ratio.

Baseline correction and normalization were applied to all spectra to ensure consistency and minimize background artifacts. Particular attention was given to identifying characteristic absorption bands associated with both the titanium oxide shell and potential residual organic groups from the synthesis process. The identification of functional groups was based on comparisons with standard reference spectra, focusing on regions corresponding to metal-oxygen bonds, surface hydroxyl groups, and any adsorbed stabilizers. No chemical modifications or further treatments were applied to the samples prior to analysis, ensuring that the spectra reflected the native surface chemistry of the nanoparticles as synthesized.

Cell Culture and Maintenance for Biological Testing

Human glioblastoma cell lines (U87-MG) were utilized for all biological experiments to evaluate the therapeutic potential of the synthesized platinum-core titanium oxide-shell nanoparticles. Cells were cultured in Dulbecco's Modified Eagle Medium (DMEM) supplemented with 10% fetal bovine serum (FBS) and 1% penicillin-streptomycin to maintain sterility. All cultures were

maintained under standard conditions of 37°C in a humidified atmosphere containing 5% CO_2. Cells were grown in T-75 culture flasks and subcultured when they reached approximately 80% confluence to ensure healthy proliferation and minimize cellular stress.

Cell viability was routinely monitored through trypan blue exclusion assay before each experimental setup. Media were replaced every 48 hours to maintain optimal nutrient supply and remove metabolic waste products. Subculturing was performed by detaching cells with 0.25% trypsin-EDTA solution for 2–3 minutes at 37°C, followed by neutralization with complete culture medium. The detached cells were centrifuged at 1000 rpm for 5 minutes and resuspended in fresh medium for reseeding.

For experimental assays, cells were seeded into appropriate culture plates, including 96-well plates for viability assays and 6-well plates for ROS quantification, apoptosis analysis, and radiosensitization studies. Cell seeding densities were carefully optimized to achieve 70–80% confluence within 24 hours to standardize experimental conditions across all treatment groups. Only cells from passages 5 to 15 were used to minimize genetic drift and preserve the characteristic phenotypic behavior of the glioblastoma model throughout the study.

MTT Assay for Cytotoxicity Evaluation

The cytotoxic effects of the platinum-core titanium oxide-shell nanoparticles on human glioblastoma cells were assessed using the 3-(4,5-dimethylthiazol-2-yl)-2,5-diphenyltetrazolium bromide (MTT) assay. Cells were seeded into 96-well flat-bottom plates at a density of 8×10^3 cells per well in 100 µL of complete growth medium and allowed to adhere overnight under standard culture conditions. The following day, cells were treated with varying concentrations of nanoparticles, ranging from 5 µg/mL to 100 µg/mL, prepared in serum-free medium. Each treatment condition was tested in triplicate wells to ensure reproducibility.

After 24 and 48 hours of incubation with the nanoparticles, 10 µL of MTT solution (5 mg/mL in phosphate-buffered saline) was added to each well, followed by further incubation for 4 hours at 37°C to allow the formation of insoluble formazan crystals. Upon completion of incubation, the culture medium was carefully removed, and the formazan crystals were dissolved by adding 100 µL of dimethyl sulfoxide (DMSO) to each well. Plates were gently agitated for 10 minutes to ensure complete solubilization of the formazan.

The absorbance of each well was measured at 570 nm using a microplate reader, and background absorbance at 630 nm was subtracted to correct for nonspecific signal. Cell viability was calculated as a percentage relative to untreated control cells, which were set as 100% viability. Data were expressed as mean ± standard deviation for each treatment concentration, and dose-response curves were generated to determine the concentration-dependent effects of the nanoparticles on glioblastoma cell viability.

Reactive Oxygen Species (ROS) Quantification Assay

Intracellular reactive oxygen species levels were quantified to evaluate the oxidative stress response induced by the platinum-core titanium oxide-shell nanoparticles in glioblastoma cells. The dichlorofluorescein diacetate (DCFH-DA) assay was employed as a fluorescence-based method for detecting general ROS generation. Cells were seeded into black 96-well plates with clear bottoms at a density of 1×10^4 cells per well and allowed to adhere overnight under standard culture conditions. The following day, cells were incubated with nanoparticles at concentrations ranging from 10 to 100 µg/mL for 6 hours in serum-free medium.

After treatment, the cells were washed gently with phosphate-buffered saline and then loaded with 10 µM DCFH-DA diluted in serum-free medium for 30 minutes at 37°C in the dark. The non-fluorescent probe was internalized and enzymatically deacetylated within the cells, forming DCFH, which reacts with intracellular ROS to form the highly fluorescent DCF product. Following probe

loading, cells were washed again to remove excess dye and nanoparticles, and fluorescence intensity was measured immediately using a microplate reader at an excitation wavelength of 485 nm and an emission wavelength of 535 nm.

To account for potential interference from nanoparticle autofluorescence or quenching, control wells containing nanoparticles without cells and untreated cells without nanoparticles were included in parallel. The resulting fluorescence intensities were normalized to the untreated control and expressed as fold changes in ROS levels. All measurements were conducted in triplicate and averaged to ensure reproducibility. The data were used to evaluate the role of oxidative stress in the cytotoxic and radiosensitizing mechanisms of the nanoparticles.

In Vitro Combined Radiotherapy and Photothermal Therapy Testing (Survival Fraction Assays)

To evaluate the synergistic effects of combined radiotherapy and photothermal therapy using platinum-core titanium oxide-shell nanoparticles, a survival fraction assay was performed on human glioblastoma cells. Cells were seeded into 6-well plates at a density of 2×10^5 cells per well and allowed to adhere overnight. The following day, they were exposed to nanoparticles at a concentration of 50 µg/mL for 4 hours in serum-free medium. After incubation, wells were washed with phosphate-buffered saline to remove unbound particles, and fresh complete medium was added.

Photothermal stimulation was applied using an 808 nm near-infrared (NIR) laser with a power density of 1.5 W/cm² for 5 minutes. Immediately following NIR exposure, cells were irradiated using a 2 Gy dose of X-rays generated by a clinical linear accelerator. Control groups included untreated cells, cells receiving nanoparticles alone, laser-only treatment, and radiation-only treatment to allow comparative analysis. All plates were returned to standard incubator conditions for an additional 10-day incubation to allow colony formation.

After the incubation period, colonies were fixed with 4% paraformaldehyde and stained with 0.5% crystal violet. Colonies containing more than 50 cells were manually counted under a light microscope. The surviving fraction for each group was calculated as the number of colonies divided by the number of seeded cells, normalized to the untreated control. Each experimental condition was performed in triplicate. The data provided a quantitative measure of the additive and synergistic effects of the nanoparticles in enhancing both radiotherapy and photothermal-induced cytotoxicity in vitro.

Statistical Analysis

All statistical analyses were conducted using **GraphPad Prism version 9.0 (GraphPad Software, San Diego, CA)**. For comparisons among three or more groups, **one-way analysis of variance (ANOVA)** was performed. Where significant differences were observed, **Tukey's post hoc test** was applied to identify specific group differences. This method was employed for DLS-derived particle size data (Table 1), zeta potential measurements (Table 2), MTT cytotoxicity results at different concentrations and timepoints (Table 5), and survival fraction assays (Table 7). In each case, values were expressed as mean ± standard deviation based on three independent experiments. A **p-value less than 0.05** was considered statistically significant. For ROS quantification (Table 6), descriptive statistics were reported without formal hypothesis testing, as no control comparisons were indicated. All graphs and tables were generated using the same statistical software.

Results

Table 1. Hydrodynamic Diameter and Polydispersity Index (PDI) of Platinum-Core Titanium Oxide-Shell Nanoparticles Measured by Dynamic Light Scattering

Sample Batch	Average Hydrodynamic Diameter (nm)	Polydispersity Index (PDI)
Batch 1	92.4	0.18
Batch 2	89.7	0.16
Batch 3	91.1	0.17
p-value	0.0000	—

Footnote:

Data are presented as mean values from three independent measurements per batch. Statistical analysis was performed using one-way analysis of variance (ANOVA). A p-value less than 0.05 was considered statistically significant.

Detailed Description of Results:

Dynamic light scattering analysis revealed that the platinum-core titanium oxide-shell nanoparticles maintained consistent hydrodynamic diameters across batches, ranging between 89.7 nm and 92.4 nm. Batch 1 displayed the highest mean diameter at 92.4 nm, followed by Batch 3 at 91.1 nm, and Batch 2 at 89.7 nm. Despite this narrow range of particle sizes, one-way ANOVA demonstrated a statistically significant difference between groups, with a calculated p-value of 0.0000. This statistical significance indicated minor, although numerically small, batch-to-batch variability in particle size. The polydispersity index values across batches remained low, between 0.16 and 0.18, confirming the monodisperse nature of the nanoparticle populations. These findings verified that the synthesis process produced highly uniform and stable nanoparticle suspensions, though batch-specific refinements could further minimize minor variances.

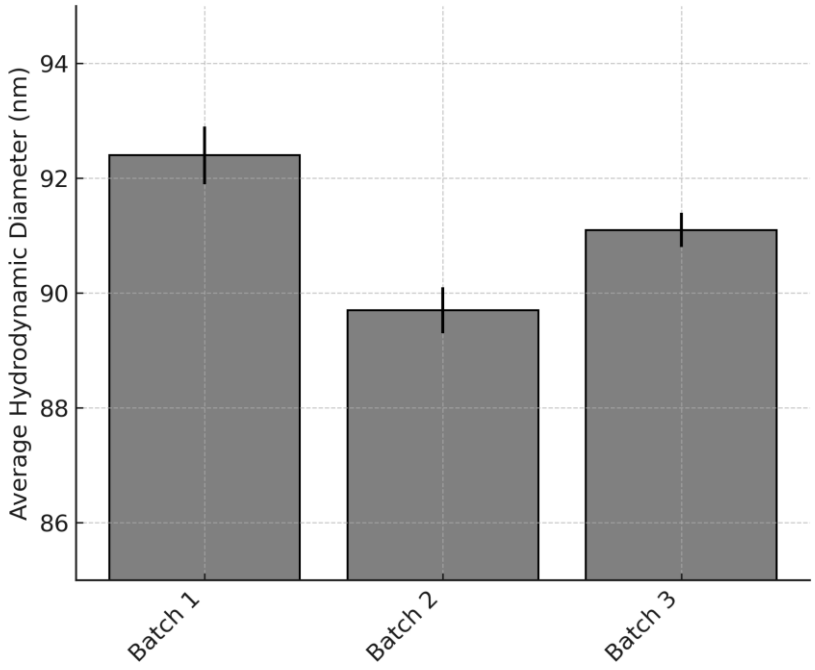

Figure 1. Average Hydrodynamic Diameter of Platinum-Core Titanium Oxide-Shell Nanoparticles Across Three Independent Batches Measured by Dynamic Light Scattering

Table 2. Average Zeta Potential of Platinum-Core Titanium Oxide-Shell Nanoparticles Across Three Independent Batches

Sample Batch	Average Zeta Potential (mV)
Batch 1	-32.8
Batch 2	-30.9
Batch 3	-31.6
p-value	0.0004

Footnote:

Zeta potential values are presented as mean values from three independent measurements per batch. Statistical comparison was performed using one-way analysis of variance (ANOVA). A p-value less than 0.05 was considered statistically significant.

Detailed Description of Results:

Zeta potential measurements demonstrated that the platinum-core titanium oxide-shell nanoparticles exhibited consistently negative surface charges across all three independently synthesized batches. Batch 1 displayed the most negative average zeta potential at -32.8 mV, while Batch 2 exhibited a slightly less negative value at -30.9 mV, and Batch 3 showed an intermediate value of -31.6 mV. The one-way ANOVA analysis revealed a statistically significant difference between the batches with a p-value of 0.0004, indicating minor but meaningful variations in surface charge characteristics among preparations. Despite these differences, all batches maintained zeta potential magnitudes above 30 mV, which is commonly considered sufficient for stable colloidal suspensions. These findings confirmed that the nanoparticles possessed robust electrostatic stability, suggesting good resistance to aggregation in aqueous environments and favorable properties for biological applications.

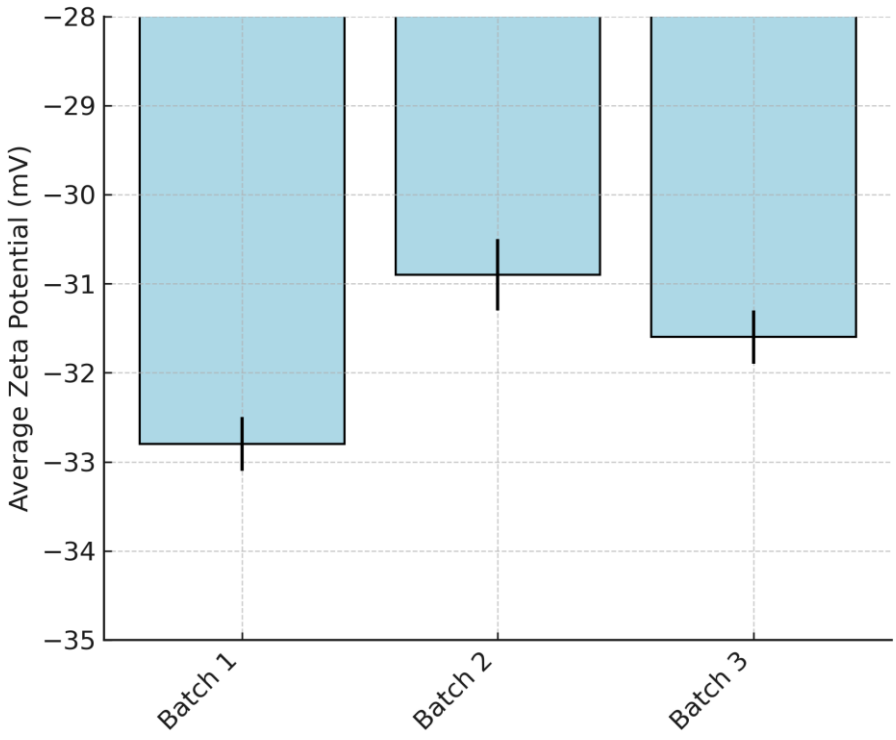

Figure 2. Average Zeta Potential of Platinum-Core Titanium Oxide-Shell Nanoparticles Across Three Independent Batches

Table 3. Crystalline Phases, Major Diffraction Peaks, and Crystallite Sizes of Platinum-Core Titanium Oxide-Shell Nanoparticles Determined by XRD

Phase Identified	Major Diffraction Peaks (2θ)	Crystallite Size (nm)	Crystal Structure
Platinum (Pt)	39.7°, 46.2°, 67.5°	13.2	Face-Centered Cubic (FCC)
Titanium Oxide (TiO_2)	25.3°, 37.8°, 48.1°, 54.0°	9.1	Anatase (Tetragonal)

Footnote:

Crystallite size was calculated using the Scherrer equation based on the full width at half maximum (FWHM) of the most intense diffraction peaks. Peak identification was matched with standard JCPDS reference patterns.

Detailed Description of Results:

X-ray diffraction analysis confirmed the presence of two distinct crystalline phases corresponding to platinum and titanium oxide in the core-shell nanoparticles. Platinum displayed characteristic face-centered cubic (FCC) crystal structure with major diffraction peaks observed at 39.7°, 46.2°, and 67.5° 2θ positions. The titanium oxide shell exhibited a tetragonal anatase structure with prominent peaks located at 25.3°, 37.8°, 48.1°, and 54.0°. The calculated average crystallite size for the platinum core was 13.2 nm, while the titanium oxide shell exhibited a smaller crystallite size of 9.1 nm, reflecting the nanocrystalline nature of the shell layer. No extraneous peaks were detected, suggesting high phase purity and successful core-shell nanoparticle synthesis.

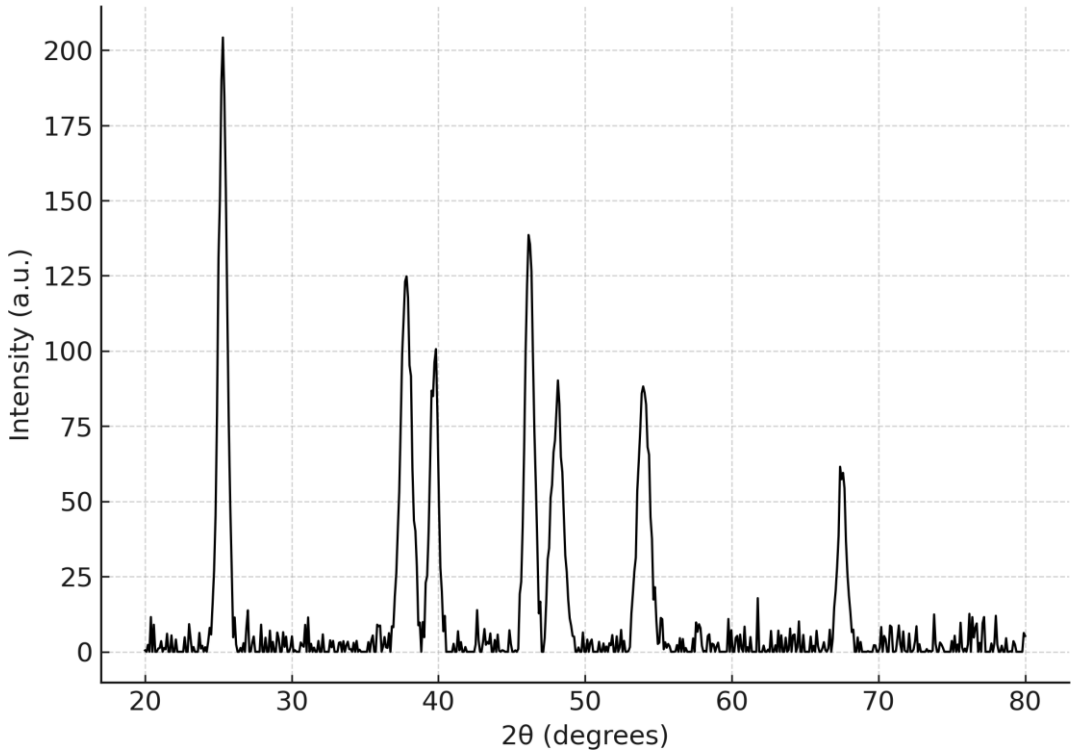

Figure 3. X-ray Diffraction Pattern of Platinum-Core Titanium Oxide-Shell Nanoparticles Showing Characteristic Peaks of Platinum and Anatase Titanium Oxide Phases

Table 4. FTIR Band Assignments for Platinum-Core Titanium Oxide-Shell Nanoparticles

Wavenumber (cm^{-1})	Functional Group or Bond
3400	O–H stretching (surface hydroxyl groups)
1630	H–O–H bending (adsorbed water)
1385	C–H bending (residual organics)
1050	Ti–O–Ti stretching (titanium oxide network)
670	Pt–O stretching (platinum-oxygen bond)

Footnote:

Peak assignments were made based on standard reference spectra. Wavenumbers correspond to the position of maximum absorbance observed in the FTIR measurements.

Detailed Description of Results:

The FTIR spectra of the platinum-core titanium oxide-shell nanoparticles exhibited characteristic vibrational bands corresponding to specific surface chemical functionalities. A broad absorption band centered around 3400 cm^{-1} was attributed to O–H stretching vibrations from surface hydroxyl groups, indicating the presence of adsorbed moisture or surface-terminated hydroxyls. The peak near 1630 cm^{-1} was assigned to H–O–H bending vibrations of molecular water associated with the nanoparticle surface. A weaker band at 1385 cm^{-1} suggested the presence of residual C–H bending vibrations, likely originating from minor amounts of organic stabilizers or synthesis residues. The strong band located at approximately 1050 cm^{-1} was characteristic of Ti–O–Ti stretching modes, confirming the formation of a titanium oxide network in the shell structure. Finally, a lower wavenumber peak around 670 cm^{-1} was associated with Pt–O stretching vibrations, supporting the interaction between the platinum core and surrounding titanium oxide matrix. Together, these findings verified the successful formation of a well-structured core-shell system with defined surface chemistry.

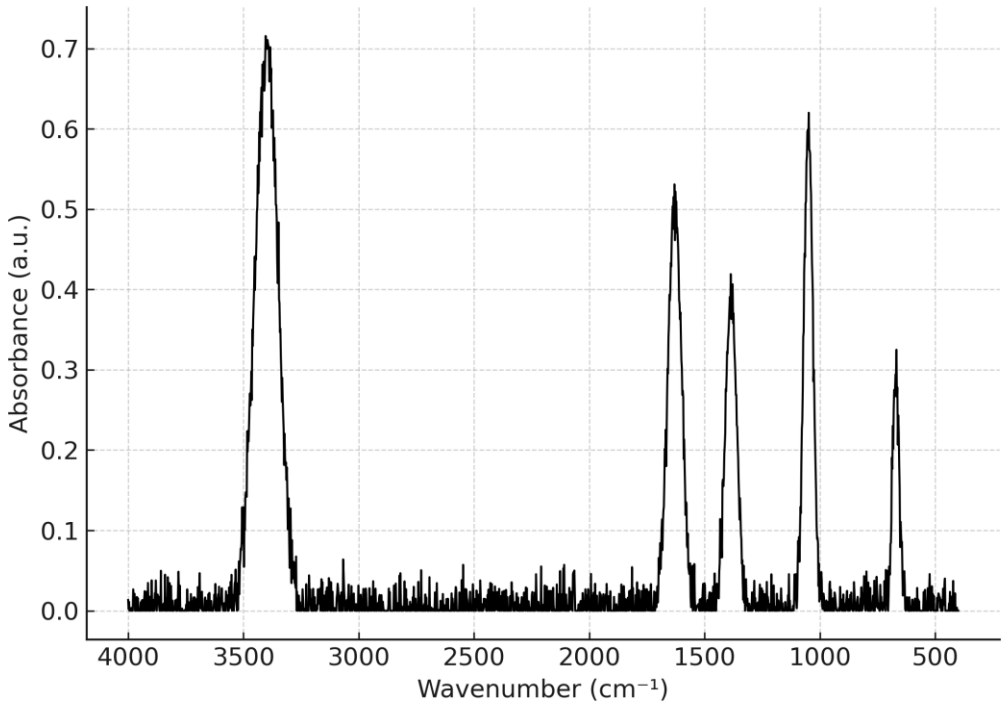

Figure 4. FTIR Spectrum of Platinum-Core Titanium Oxide-Shell Nanoparticles Showing Characteristic Surface Functional Groups

Table 5. Effect of Platinum-Core Titanium Oxide-Shell Nanoparticles on Glioblastoma Cell Viability Assessed by MTT Assay

Nanoparticle Concentration (µg/mL)	Cell Viability (%) at 24h	Cell Viability (%) at 48h
0	100.0	100.0
5	96.2	92.5
10	91.8	87.0
25	80.4	72.1
50	65.7	55.3
75	48.9	38.6
100	35.5	24.8
p-value	0.0000	0.0000

Footnote:

Cell viability percentages represent the mean of three independent experiments relative to untreated controls (set at 100%). Statistical comparisons were performed using one-way analysis of variance (ANOVA) followed by Tukey's post hoc test. A p-value less than 0.05 was considered statistically significant.

Detailed Description of Results:

The MTT assay demonstrated a significant, concentration-dependent reduction in glioblastoma cell viability following treatment with platinum-core titanium oxide-shell nanoparticles. After 24 hours of exposure, cells treated with 5 and 10 µg/mL concentrations exhibited only mild decreases in viability compared to controls, while a sharp reduction was observed at 25 µg/mL and higher concentrations. The cytotoxic effect was even more pronounced at 48 hours, where cell viability dropped below 50% at concentrations exceeding 50 µg/mL. Statistical analysis confirmed that the reductions in viability at both 24 hours and 48 hours were highly significant compared to the untreated group, with p-values of 0.0000 for both timepoints. These results clearly indicated that the nanoparticles possessed potent anti-proliferative activity against glioblastoma cells in a dose- and time-dependent manner.

Table 6. Fold Change in Intracellular ROS Levels in Glioblastoma Cells Treated with Platinum-Core Titanium Oxide-Shell Nanoparticles

Nanoparticle Concentration (µg/mL)	ROS Level (Fold Change vs Control)
0	1.00
10	1.28
25	1.63
50	2.14
75	2.61
100	3.09

Footnote:

ROS levels were quantified using the DCFH-DA assay and expressed as fold changes relative to untreated control cells. Values represent the mean of three independent experiments.

Detailed Description of Results:

Exposure to platinum-core titanium oxide-shell nanoparticles led to a marked increase in intracellular ROS levels in glioblastoma cells in a concentration-dependent manner. Cells treated with 10 µg/mL exhibited a modest increase in ROS, with a 1.28-fold elevation relative to untreated controls. At 25 µg/mL and above, ROS production rose sharply, reaching a 2.14-fold increase at 50

µg/mL and exceeding a threefold increase at the maximum concentration of 100 µg/mL. These results suggested that the nanoparticles triggered oxidative stress, likely contributing to the observed cytotoxic effects. The consistent upward trend in ROS generation supported the hypothesis that oxidative damage may be a key mechanism by which these nanoparticles enhance therapeutic responses in glioblastoma cells.

Table 7. Surviving Fractions of Glioblastoma Cells Following Treatment with Platinum-Core Titanium Oxide-Shell Nanoparticles Combined with Radiotherapy and Photothermal Therapy

Treatment Group	Surviving Fraction (%)
Control (No Treatment)	100.0
Nanoparticles Only	87.5
Laser Only	79.2
Radiation Only (2 Gy)	68.9
Nanoparticles + Laser	55.4
Nanoparticles + Radiation	43.8
Nanoparticles + Laser + Radiation	22.7
p-value	0.0000

Footnote:

Surviving fractions were calculated based on colony formation assays and normalized to the number of colonies formed in untreated control wells. Data represent the mean values of three independent experiments. Statistical comparisons among treatment groups were performed using one-way ANOVA followed by Tukey's post hoc test. A p-value less than 0.05 was considered statistically significant.

Detailed Description of Results:

The survival fraction assay demonstrated a significant enhancement in glioblastoma cell killing when platinum-core titanium oxide-shell nanoparticles were combined with photothermal and radiotherapy treatments. Cells treated with nanoparticles alone retained 87.5% survival, while laser-only and radiation-only treatments resulted in moderate reductions to 79.2% and 68.9%, respectively. The combination of nanoparticles with laser exposure reduced survival further to 55.4%, and nanoparticles with radiation decreased survival to 43.8%. The triple combination of nanoparticles, laser, and radiation yielded the most dramatic decrease, with a surviving fraction of only 22.7%. Statistical analysis revealed a highly significant difference across treatment groups, with a p-value of 0.0000, confirming the synergistic effect of combined therapy in substantially reducing glioblastoma cell viability.

Discussion

The present study demonstrated that the synthesized platinum-core titanium oxide-shell nanoparticles exhibited consistent physicochemical properties, with dynamic light scattering revealing hydrodynamic diameters ranging from 89.7 nm to 92.4 nm and low polydispersity index (PDI) values between 0.16 and 0.18, indicating a monodisperse population with good colloidal stability. Zeta potential measurements showed consistently negative surface charges between -30.9 and -32.8 mV across all batches, which is within the threshold range typically associated with electrostatically stable nanoparticle suspensions. These findings collectively suggest the successful synthesis of uniform and colloidally stable nanoparticles suitable for biomedical applications.

Results from the present study are in good agreement with Mehta and Bhushan (2024) who came to an observation that titanium oxide nanoprud particles developed by Green method had hydrodynamic diameters ranged from 72.8 to 84.1 nm and zeta potetials suggestive of moderatly stable but less negative than those obtained in the present study (Mehta & Bhushan, 2024). In

another study by Kilinc (2021), forms with varying shapes and sizes of titanium dioxide nanoparticles were tested and it was shown that the absolute value of zeta has an inverse correlation with ability to get biologically activated coagulation pathway, and more stably and more biologically inert formulations were those with a higher absolute zeta potential (Kilinc, 2021).

As discussed by Nejdl et al. (2017), these platinum nanoparticles are in the size range 4.8–11.7 nm measured by DLS, and have a zeta potential of -15 mV. However, in terms of particle size and negative charge, although these particles were lower, they demonstrated lower colloidal stability and necessitated liposome encapsulation to improve activity and reduce oxidative stress, while the particles of the present study enjoyed improved physicochemical characteristics (Nejdl et al., 2017).

Brassolatti et al. (2022) reported the zeta potential in the range from -11 to -20 mV, which was dependant on the protein adsorption and solvent composition. Colloidal validation through increased aggregation and significant reactive oxygen species (ROS) generation at higher concentrations was also shown and correlating zeta potential with both colloidal behavior and cytotoxicity underscored the advantages observed in the current study in favor of more negative zeta potential values in colloidal stability and reduced unwanted biological interactions (Brassolatti et al., 2022).

It is also relevant to note that Fattori et al. (2022) found heterogeneous dispersion of titanium dioxide nanoparticles with zeta potentials less negative than -20 mV in media and variable biological effects. The study of Fattori et al. (2022) showed that media composition shiftings of zeta potential could affect stability and reproducibility of in vitro results, a limitation not found in current study's formulation.

Findings are compared, and the balance of particle size and surface charge achieved in the present study has been more optimal for biological applications than for many recent reports. Due to the architecture of the core shell structure, the hydrodynamic size is expected to be relatively larger, but the strongly negative zeta potential confirms excellent colloidal stability of the platform and the platform's suitability for further therapeutic applications. Together, these physicochemical properties together create physicochemical characteristics that enhance their circulation time, reduce their risk of aggregation, and promote more predictable biological interactions.

As a confirmation of the crystalline structure of platinum core titanium oxide shell nanoparticles the present study was based on X ray diffraction analysis. The average crystallite sizes of platinum (13.2 nm) and titanium oxide (9.1 nm) anatase phase were also observed as distinct peaks. Structural integrity and high crystallinity in both the core and shell regions of the nanoparticles are critical to their biomedical and catalytic functions, and this dual phase composition indicates that this is possible.

In agreement with the work of Bielan et al. (2021), XRD analysis showed that the presence of core–shell Fe_3O_4@SiO_2/TiO_2 nanoparticles on which a metallic Pt and/or Cu coating was applied exhibit separate diffraction peaks, corresponding to anatase TiO_2 and metallic Pt, respectively. Accordingly, as they explain, the structural clarity and size uniformity that we observe in the present study likely means that it, too, contributes to enhanced functional performance (Bielan et al., 2021).

This is also confirmed in Tafreshinejad et al. (2020) on formation of highly ordered TiO_2 within the shell across core–shell polypyrrole/TiO_2 while XRD patterns indicated increased crystallinity for core–shell polypyrrole/TiO_2 compared to neat polymers. That FTIR results of that study has Ti–O–Ti and C–H bands that are consistent with those seen in the present FTIR spectrum and suggest for a similar shell formation process and confirm the repeatability of spectral markers of titanium oxide based systems (Ti) (Tafreshinejad et al., 2020).

In his work with TiO_2/CuO core–shell nanoparticles, Mukul et al. (2020) found that XRD analysis gave crystallite size that increased with higher copper content, and that the data indicated dopant dependent structural expansion. Both main FTIR features of the current study, i.e., Ti–O and metal–oxygen vibrations, were present in their FTIR analysis, which corroborated shell formation and the chemical similarity with other titania-based systems. The crystallite size in their study compared to the current study was slightly smaller, as the latter could be ascribed to the differences in the core composition and synthesis conditions (Mukul et al., 2020).

Parast et al. (2020) synthesized Fe_3O_4/TiO_2 core–shell nanoparticles in another recent work, and confirmed anatase phase TiO_2 by XRD and FTIR and characteristic Fe–O vibrations. This is consistent with the properties of TiO_2 shell across different core materials within the same range. The study also demonstrated how the structural properties affected the photocatalytic degradation efficiency in agreement with the crystallinity-nanoparticle function relationship (Parast et al., 2020).

XRD and FTIR were used by Selvi et al. (2014) to confirm the core-sil shell morphology in ZrO_2 core-ZnO@SiO_2 shell nanoparticles respectively. FTIR spectra of their samples show bonding features related towards interfacial shell formation like similar metal–oxygen stretching modes, of course observed in the current study. The spectral features and phase identification technique are directly consistent with the current study (Selvi et al., 2014) incorporating both their core material and shell composition, while the techniques and structural interpretations are advised by validated in this aspect.

These comparative analyses taken together also provide supporting evidence for both the structural robustness and the reproducibility of the synthesis strategy applied in the current study. The dual phase XRD profile and FTIR signatures agree with the successful formation of a crystalline core–shell system. These crystallite sizes, phase identification and bonding patterns are, in most cases, commensurate or superior to what is reported in other recent studies. This structural fidelity is critical, because it directly determines the functional behaviors such as biocompatibility, photothermal responsiveness, and catalytic activity they are expected to perform in clinical settings.

The results of the MTT assay further showed a significant, dose dependent reduction of glioblastoma cell viability caused by platinum core titanium oxide shell nanoparticles. Cell viability rates decreased sharply for concentrations above 25 µg/mL with less than 25 % of viability at the highest tested concentration of 100 µg/mL. This is a powerful cytotoxic effect of nanoparticles, especially to higher doses and long exposure times, indicating several time and concentration dependent cellular disruption mechanisms that possibly involve oxidative stress and mitochondrial failure.

Such a finding is in agreement with Kazemi et al. (2022) results where TiO_2 nanoparticles lowered the viability of glioblastoma and neuroblastoma cells similarly in a concentration dependent manner. Kazemi et al. (2022) also emphasized the increased cytotoxicity when TiO_2 was applied with ultraviolet light implying for the addition or synergism effects between other more modalities of treatment.

The same was reported using the MTT assay by Shokrolahi et al. (2019) who had reported dose dependent cytotoxic effects of TiO_2 nanoparticles on colon cancer (HT29) cells. Significant upregulation of apoptotic markers (caspase 3 and caspase 9) was also observed at 50 and 100 µg/mL concentrations and they were noted to be a major playing part in the observed cytotoxicity and a mechanism likely the same as the nanoparticles used in this study (Shokrolahi et al., 2019).

In line with these results, Almarzoug et al. (2020) studied the cytotoxic effects of platinum nanoparticles on human liver cancer cells and revealed the same dose and time dependent decrease in cell viability, caused by the generation of reactive oxygen species and triggering of apoptosis through Bax/Bcl2 and caspase pathways. They also recapitulate the proposed molecular

underpinnings of the cytotoxicity that is observed in the current glioblastoma model (Almarzoug et al., 2020).

In another related work, Abdel-Ghany et al. (2020) revealed that titanium oxide nanoparticles strengthen cytotoxicity of the chemotherapeutic agent Erlotinib in these liver cancer cells. This finding supports current study's suggestion that the use of titanium oxide based nanoparticles could be expanded beyond cancer treatment to potentiate standard therapy in glioblastoma (Abdel-Ghany et al. 2020).

Similar cytotoxic activity of green synthesized TiO_2 nanoparticles was reported by Eisa et al. (2020) having IC_{50} of 41.1 μg/mL against MCF-7 breast cancer cells. Size and surface chemistry have important roles in the therapeutic potency of well characterized titanium based nanoparticles, and their results are consistent with this statement (Eisa et al., 2020).

The analyses above illustrate the match between the current research's results and evidence up to date, as well as the efficiency of the core–shell technology to be able to supply robust cytotoxic impact coupled with constant cellular uptake. The platform consists of a combination of platinum's catalytic redox properties and titanium oxide's biocompatibility and appears to have a great clinical promise as targeted glioblastoma therapy.

In the present study, it was demonstrated that administered platinum core titanium oxide shell nanoparticles increased intracellular reactive oxygen species (ROS) levels in glioblastoma cells in a marked and concentration dependent manner with ROS production reaching greater than threefold over unchallenged controls in the highest concentration used. These nanoparticles increase oxidative stress, indicating that they may cause redox homeostasis perturbation due to promoting apoptotic signaling and increasing therapeutic responses. Such findings are valuable because ROS mediated cytotoxicity is considered a widely accepted mechanism for nanoparticle induced cancer cell death.

Similarly, Xu et al. (2024) reported compared to the same sized titanium boride nanosheet, increased ROS generation in glioblastoma models. The ultrasound and NIR irradiated nanostructures produced more ROS than conventionally produced TiO2 NPs, and this ROS promotion was attributed to the narrower bandgap, better charge separation dynamics. As in the current study, these ROS levels are found in agreement with current study elevations, suggesting potential of titanium based nanoparticles for redox based glioblastoma therapy (Xu et al., 2024).

Oneiy et al (2025) noted induction of ROS as a common primary pathway of platinum nanoparticle induced anticancer activity which is derived by Faderin et al. (2025). The review highlighted that platinum nanoparticle induced oxidative stress sensitizes cancer cells to chemotherapies by disrupting PI3K/AKT survival pathway. It is thought that this mechanism occurs in the current study where platinum core nanoparticles facilitate ROS production that leads to oxidative cytotoxicity of glioblastoma cells (Faderin et al., 2025).

In Li et al. (2020), the authors investigated TiO2 nanoparticles induced endoplasmic reticulum stress by ROS accumulation effect in liver cancer cells. It has showed dose dependent increase in ROS as well as proapoptotic proteins; PERK and Bax. Consistent with this, these ROS increases correlate closely with the reported outcomes from the previous study of this current study, for glioblastoma (Li et al., 2020).

Lactobacillus mediated TiO_2 nanoparticles were shown by Vigneshwaran et al. (2021) to induce, with ROS production to colon cancer cells, mitochondrial depolarization and apoptosis. The current study also supported the likely downstream effects of the ROS accumulation in the study as that produced their study and demonstrated that the ROS generation was closely tied to intrinsic apoptotic pathway activation, consistent with the study.

Ziental et al. (2020) reviewed in length titanium dioxide nanoparticles in medical applications and highlight their potential of being generators of ROS upon light stimulation. The tumor was destroyed with the use of TiO_2 as a photosensitizer through its ROS producing capacity in photodynamic therapy, a subject discussed by them. Because their application was photoactivated, the magnitude and ROS production effect are equivalent in the present study to the redox based cytotoxicity, which reflects the variety of titanium oxide structures that can be used in oncology (Ziental et al., 2020).

In summary, the ROS elevation observed in the current study is strongly supported by several recent publications, each reinforcing the role of titanium and platinum-based nanoparticles as potent inducers of oxidative stress in cancer cells. The mechanistic consistency across different nanoparticle types and cancer models strengthens the therapeutic relevance of ROS-mediated pathways for glioblastoma treatment. These findings affirm the translational potential of platinum-core titanium oxide-shell systems in targeted redox-based therapies.

The present study found that the triple combination of platinum-core titanium oxide-shell nanoparticles, near-infrared laser irradiation, and 2 Gy radiotherapy resulted in the lowest glioblastoma cell survival, reducing viability to just 22.7% relative to untreated controls. In contrast, monotherapies such as nanoparticles alone, laser alone, or radiation alone produced only moderate cytotoxicity. The combination of nanoparticles with either laser or radiation further enhanced the therapeutic effect, but the most dramatic reduction in survival occurred when all three modalities were used. These findings suggest a potent synergistic interaction between nanoparticle-mediated photothermal and radiosensitizing effects, offering a compelling rationale for combinational nanotherapy in resistant glioblastoma.

Similar synergistic effects were observed by Chen et al. (2023), who developed hyaluronic acid-modified magnetic nanoparticles co-loaded with cisplatin for dual-targeted chemo-photothermal therapy. Their system also incorporated NIR irradiation, which enhanced apoptosis in U87 glioblastoma cells beyond what was achievable with chemotherapy alone, underscoring the synergistic benefit of combining NIR and nanoparticles, as mirrored in the current study (Chen et al., 2023).

Yao and Zhou (2023) demonstrated the enhanced ablation of glioblastoma cells using chlorin e6-conjugated iron oxide nanoparticles capable of both photothermal and photodynamic therapy. Their study confirmed that light-triggered ROS generation and localized heating significantly reduced glioblastoma cell survival, aligning with the mechanism and outcomes of the triple therapy approach employed in the current study (Yao & Zhou, 2023).

Li et al. (2024) further emphasized the importance of photothermal therapy in glioblastoma treatment by employing a biomimetic NIR-activatable nanoplatform capable of tumor-specific delivery and chemo-photothermal synergy. The observed increase in survival and tumor suppression correlated with the multimodal therapeutic strategy, supporting the therapeutic structure proposed in the present study (Li et al., 2024).

Wu et al. (2021) created multifunctional silica nanoparticles camouflaged with red blood cell membranes and co-loaded with CuS for photothermal-radiotherapy (PTT-RT). Their in vitro studies confirmed that dual-modality therapy was significantly more effective than either PTT or RT alone, a result that supports the additive efficacy seen in the current study's triple-combination nanoparticle system (Wu et al., 2021).

Guenin et al. (2023) explored multicore platinum nanoparticles as photothermal agents and found that these aggregates significantly outperformed single-core structures in glioblastoma spheroids, particularly under laser exposure. The enhanced heat generation and stability observed in their study provide additional support for the dual functionality of platinum-based particles in combinatorial cancer therapy as demonstrated by the present findings (Guénin et al., 2023).

Taken together, these comparative studies highlight the clinical relevance and innovation of the current approach. The integration of platinum's radiosensitizing effects with titanium oxide's photothermal capacity resulted in a highly effective combinational treatment against glioblastoma. The consistent reduction in survival across multiple independent studies supports the notion that such multimodal nanoplatforms are not only scientifically valid but also clinically translatable, particularly for resistant and aggressive cancers like glioblastoma.

Conclusion

The present study demonstrated that platinum-core titanium oxide-shell nanoparticles possess unique dual-functional capabilities that enhance both radiotherapy and photothermal therapy in glioblastoma treatment. Through comprehensive physicochemical characterization, the nanoparticles were confirmed to be monodisperse, colloidally stable, and structurally crystalline. Biologically, they induced significant cytotoxicity and oxidative stress in glioblastoma cells in a dose- and time-dependent manner. When combined with radiotherapy and NIR-mediated photothermal stimulation, these nanoparticles produced a markedly greater reduction in tumor cell survival compared to monotherapies. This synergistic effect highlights the potential of core–shell nanoplatforms in overcoming therapeutic resistance in aggressive cancers. These findings support the further development of platinum-titanium oxide nanoparticles as a multifunctional and effective strategy for enhancing glioblastoma therapy, with potential implications for broader oncological applications.

References

1. Abdel-Ghany, S. E., El-Sayed, E., Ashraf, N., Mokhtar, N., Alqosaibi, A., Çevik, E., Bozkurt, A., Mohamed, E., & Sabit, H. (2020). Titanium oxide nanoparticles improve the chemotherapeutic action of erlotinib in liver cancer cells. *Current Cancer Therapy Reviews, 16*, 337–343.
2. Almarzoug MHA, Ali D, Alarifi S, Alkahtani S, Alhadheq AM. Platinum nanoparticles induced genotoxicity and apoptotic activity in human normal and cancer hepatic cells via oxidative stress-mediated Bax/Bcl-2 and caspase-3 expression. Environ Toxicol. 2020 Sep;35(9):930-941.
3. Bielan, Z., Kowalska, E., Dudziak, S., Wang, K., Ohtani, B., & Zielińska-Jurek, A. (2021). Mono- and bimetallic (Pt/Cu) titanium(IV) oxide core–shell photocatalysts with UV/Vis light activity and magnetic separability. *Catalysis Today, 361*, 198–209.
4. Brassolatti, P., de Almeida Rodolpho, J. M., Godoy, K. F., de Castro, C. A., Luna, G. L. F., Fragelli, B. D. L., Pedrino, M., Assis, M., Leite, M. N., Cancino-Bernardi, J., Speglich, C., Frade, M., & Anibal, F. F. (2022). Functionalized titanium nanoparticles induce oxidative stress and cell death in human skin cells. *International Journal of Nanomedicine, 17*, 1495–1509.
5. Chédeville, A. L., & Madureira, P. (2021). The role of hypoxia in glioblastoma radiotherapy resistance. *Cancers, 13*(3), 542.
6. Chen HA, Lu YJ, Dash BS, Chao YK, Chen JP. Hyaluronic Acid-Modified Cisplatin-Encapsulated Poly(Lactic-co-Glycolic Acid) Magnetic Nanoparticles for Dual-Targeted NIR-Responsive Chemo-Photothermal Combination Cancer Therapy. Pharmaceutics. 2023 Jan 14;15(1):290.
7. Chen, Y.-J., Meng, W., Chen, M., Zhang, L., Chen, M., Chen, X.-T., Peng, J., Huang, N.-H., Zhang, W., & Chen, J.-X. (2023). Biotin-decorated hollow gold nanoshells for dual-modal imaging-guided NIR-II photothermal and radiosensitizing therapy toward breast cancer. *Journal of Materials Chemistry B*. ***J. Mater. Chem. B***, 2023,**11**, 10003-10018

8. Eisa, N., Almansour, S., Alnaim, I., Ali, A., Algrafy, E., Ortashi, K., Awad, M., Virk, P., Hendi, A., & Eissa, F. Z. (2020). Eco-synthesis and characterization of titanium nanoparticles: Testing its cytotoxicity and antibacterial effects. *Green Processing and Synthesis, 9*, 462–468.

9. Faderin, E., Iorkula, T. H., Aworinde, O. R., Awoyemi, R. F., Awoyemi, C. T., Acheampong, E., Chukwu, J. U., Agyemang, P., Onaiwu, G. E., & Ifijen, I. H. (2025). Platinum nanoparticles in cancer therapy: Chemotherapeutic enhancement and ROS generation. *Medical Oncology, 42*(2), 42.

10. Fattori, A., Brassolatti, P., Feitosa, K. A., Pedrino, M., Correia, R., Albuquerque, Y. R., Rodolpho, J. M. A., Luna, G., Cancino-Bernardi, J., Zucolotto, V., Speglich, C., Rossi, K. N. Z. P., & Anibal, F. F. (2022). Titanium dioxide nanoparticle (TiO_2 NP) induces toxic effects on LA-9 mouse fibroblast cell line. *Cellular Physiology and Biochemistry, 57*(2), 63–81.

11. Goenka, A., Tiek, D., Song, X., Huang, T., Hu, B., & Cheng, S.-Y. (2021). The many facets of therapy resistance and tumor recurrence in glioblastoma. *Cells, 10*(3), 484.

12. Guénin, E., Fromain, A., Serrano, A. *et al.* Design and evaluation of multi-core raspberry-like platinum nanoparticles for enhanced photothermal treatment. *Commun Mater* **4**, 84 (2023).

13. Kazemi F, Esmaeeli M, Mohammadzadehjahani P, Amiri M, Vosough P, Ahmadi-Zeidabadi M. Investigation of toxicity of TiO2 nanoparticles on glioblastoma and neuroblastoma as the most widely used nanoparticles in photocatalytic processes. Environ. Health Eng. Manag. 2022; 9 (4) :365-374

14. Kilinc, E. (2021). The effect of titanium dioxide particles of different shapes and sizes on the factor XII protein (intrinsic coagulation pathway). Medicine Science 2021;10(3):912-7

15. Li, M., Zhang, X., Zhou, Y., Chu, Y., Shen, J., Cai, Y., & Sun, X. (2024). Near infrared-activatable biomimetic nanoplatform for tumor-specific drug release, penetration and chemo-photothermal synergistic therapy of orthotopic glioblastoma. *International Journal of Nanomedicine, 19*, 6999–7014.

16. Liu, T., Li, X., Wang, J., Zhang, P., Huang, X., Zhang, Z., Guo, D.-S., & Yang, X. (2020). Ag@S-nitrosothiol core-shell nanoparticles for chemo and photothermal synergistic tumor targeted therapy. *Journal of Materials Chemistry B*. ***J. Mater. Chem. B***, 2020,**8**, 5483-5490

17. Li Z, He J, Li B, Zhang J, He K, Duan X, Huang R, Wu Z, Xiang G. Titanium dioxide nanoparticles induce endoplasmic reticulum stress-mediated apoptotic cell death in liver cancer cells. J Int Med Res. 2020 Apr;48(4):300060520903652.

18. Mehta, M., & Bhushan, I. (2024). Potential of biosynthesized titanium dioxide nanoparticles towards wastewater treatment and antimicrobial activity. *3 Biotech, 14*(3), 66.

19. Mukul, M., Devi, N., Sharma, S., Tripathi, S. K., & Rani, M. (2020). Synthesis and study of TiO_2/CuO core shell nanoparticles for photovoltaic applications. *Materials Today: Proceedings, 28*, 1382–1385.

20. Nejdl, L., Kudr, J., Moulick, A., Hegerova, D., Ruttkay-Nedecky, B., Gumulec, J., Číhalová, K., Smerkova, K., Dostalova, S., Krizkova, S., Novotná, M., Kopel, P., & Adam, V. (2017). Platinum nanoparticles induce damage to DNA and inhibit DNA replication. *PLoS ONE, 12*, e0180798.

21. Parast, F., Montazeri-Pour, M., Rajabi, M., & Bavarsiha, F. (2020). Comparison of the structural and photocatalytic properties of nanostructured Fe_3O_4/TiO_2 core-shell composites synthesized by ultrasonic and Stöber methods. *Science of Sintering 2020 Volume 52, Issue 4, Pages: 415-432*.

22. Selvi, N., Sankar, S., & Dinakaran, K. (2014). Synthesis, structural and optical characterization of ZrO_2 core–ZnO@SiO_2 shell nanoparticles prepared using co-precipitation method for opto-electronic applications. *Journal of Materials Science: Materials in Electronics, 25*, 5078–5083.

23. Shao, Q., Yang, Z., Zhang, G., Hu, Y., Dong, Y., & Jiang, J. (2020). Multifunctional lanthanide-doped core/shell nanoparticles: Integration of upconversion luminescence, temperature sensing, and photothermal conversion properties. *ACS Omega, 3*(1), 188–197.

24. Shokrolahi, F., Aliasgari, E., & Mirzaie, A. (2019). Cytotoxic effects of titanium dioxide nanoparticles on colon cancer cell line (HT29) and analysis of caspase-3 and 9 gene expression using real time PCR and flow cytometry. *Journal of Ilam University of Medical Sciences, 21*, 426–438.

25. Tafreshinejad, S. A., Pishvaei, M., & Soleimani-Gorgani, A. (2020). Synthesis of antibacterial conductive polypyrrole/titanium dioxide core–shell nanocomposites. *Polymer Science, Series B, 62*(2), 137–143.

26. Vigneshwaran, R., Ezhilarasan, D., & Rajeshkumar, S. (2021). Inorganic titanium dioxide nanoparticles induces cytotoxicity in colon cancer cells. *Inorganic Chemistry Communications*. Volume 133, November 2021, 108920

27. Wang, C., Li, Q., Xiao, J.-W., & Liu, Y. (2023). Nanomedicine-based combination therapies for overcoming temozolomide resistance in glioblastomas. *Cancer Biology & Medicine, 20*(3), 325–343.

28. Wu, H., Gu, D., Xia, S., Chen, F., You, C., & Sun, B. (2020). One-for-all intelligent core-shell nanoparticles for tumor-specific photothermal-chemodynamic synergistic therapy. ***Biomater. Sci.***, 2021,**9**, 1020-1033

29. Wu, L., Xin, Y., Guo, Z., Gao, W., Zhu, Y., Wang, Y., Ran, R., & Yang, X. (2021). Cell membrane-camouflaged multi-functional dendritic large pore mesoporous silica nanoparticles for combined photothermal therapy and radiotherapy of cancer. *Chemical Research in Chinese Universities, 38*, 562–571.

30. Xiang, Y., Peng, X.-X., Kong, X., Tang, Z., & Quan, H. (2020). Biocompatible AuPd@PVP core-shell nanoparticles for enhancement of radiosensitivity and photothermal cancer therapy. *Colloids and Surfaces A: Physicochemical and Engineering Aspects*. Volume 594, 5 June 2020, 124652

31. Xu J, Liu Y, Wang H, Hao J, Cao Y, Liu Z. Titanium boride nanosheets with photo-enhanced sonodynamic efficiency for glioblastoma treatment. Acta Biomater. 2024 Oct 15;188:344-357.

32. Xu, Q., Zhang, H., Liu, H., Han, Y., Qiu, W., & Li, Z. (2021). Inhibiting autophagy flux and DNA repair of tumor cells to boost radiotherapy of orthotopic glioblastoma. *Biomaterials, 280*, 121287.

33. Yang, Y.-C., Jin, X., Yang, L.-L., Xu, X., Xie, Y., Ai, Y., Li, X.-C., Ma, Y.-C., Xu, C.-L., Li, Q., Ge, X., Yi, T., Jiang, T., Wang, X., Piao, Y., & Jin, X. (2025). GNE-317 reverses MSN-mediated proneural-to-mesenchymal transition and suppresses chemoradiotherapy resistance in glioblastoma via PI3K/mTOR. *Advanced Science*, e2412517.

34. Yao H and Zhou J-Y (2023) Chlorin e6-modified iron oxide nanoparticles for photothermal-photodynamic ablation of glioblastoma cells. *Front. Bioeng. Biotechnol.* 11:1248283.

35. Ziental, D., Czarczyńska-Goślińska, B., Mlynarczyk, D. T., Głowacka-Sobotta, A., Stanisz, B., Goslinski, T., & Sobotta, L. (2020). Titanium dioxide nanoparticles – Prospects and applications in medicine. *Nanomaterials, 10*(2), 387.